pubs.acs.org/Biomac

Article

pH-Responsive Amphiphilic Polyether Micelles with Superior Stability for Smart Drug Delivery

Iloh Son, Yujin Lee, Jinsu Baek, Miran Park, Daeho Han, Seung Kyu Min, Dongwon Lee, and Byeong-Su Kim*

Cite This: *Biomacromolecules* 2021, 22, 2043−2056

Read Online

ACCESS | Metrics & More | Article Recommendations | Supporting Information

ABSTRACT: Despite widespread interest in the amphiphilic polymeric micelles for drug delivery systems, it is highly desirable to achieve high loading capacity and high efficiency to reduce the side effects of therapeutic agents while maximizing their efficacy. Here, we present a novel hydrophobic epoxide monomer, cyclohexyloxy ethyl glycidyl ether (CHGE), containing an acetal group as a pH-responsive cleavable linkage. A series of its homopolymers, poly(cyclohexyloxy ethyl glycidyl ether)s (PCHGEs), and block copolymers, poly(ethylene glycol)-*block*-poly(cyclohexyloxy ethyl glycidyl ether)s (*m*PEG-*b*-PCHGE), were synthesized via anionic ring-opening polymerization in a controlled manner. Subsequently, the self-assembled polymeric micelles of *m*PEG-*b*-PCHGE demonstrated high loading capacity, excellent stability in biological media, tunable release efficiency, and high cell viability. Importantly, quantum mechanical calculations performed by considering prolonged hydrolysis of the acetal group in CHGE indicated that the CHGE monomer had higher hydrophobicity than three other functional epoxide monomer analogues developed. Furthermore, the preferential cellular uptake and *in vivo* therapeutic efficacy confirmed the enhanced stability and the pH-responsive degradation of the amphiphilic block copolymer micelles. This study provides a new platform for the development of versatile smart polymeric drug delivery systems with high loading efficiency and tailorable release profiles.

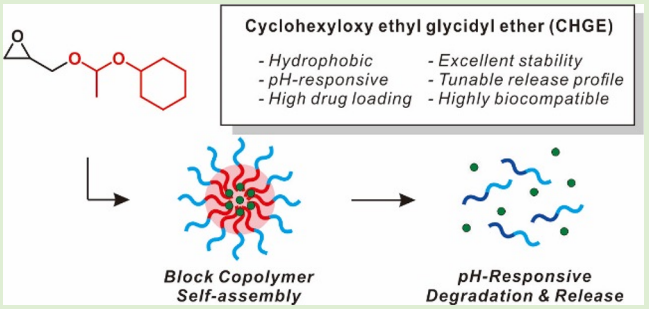

INTRODUCTION

Chemotherapy is the most common means to treat cancer. For this purpose, it is highly desirable to develop a novel drug delivery system with improved efficiency to overcome the intrinsic limitations of therapeutic agents, such as high toxicity, fast clearance, and poor tumor selectivity. To address these challenges, there have been significant advances in the development of polymeric drug carriers, including polymer drug conjugates, liposomes, and polymeric micelles.[1−3] Among these, polymeric micelles have been widely employed as ideal drug delivery carriers owing to their unique advantages such as highly tunable loading efficiency and capacity, facile modification, long circulation time in the circulatory system, and tunable degradation kinetics.[4,5]

Despite these advantages and the significant progress made in achieving efficient drug delivery, the stability of polymeric micelles has been the primary challenge for further applications.[6] In particular, the stability of drug carriers in a biological environment is important.[7] The adsorption of various proteins or components by drug carriers upon coming in contact with biological media adversely affects the stability and efficiency of the drug carriers.[8] Moreover, the stability of polymeric micelles in the bloodstream is reduced because of the dynamic shuttling of polymer chains between the micelles and bulk phase.[9] These challenges have been addressed by exploiting noncovalent interactions, such as hydrophobic,[10] electrostatic,[11] host−guest,[12] hydrogen bonding,[13] stereocomplex,[14] and coordination interactions,[15] in polymeric micelles. Among these interactions, hydrophobic interactions are known to strongly influence the stability and loading efficiency of the micelles. As notable examples, Li et al. synthesized reduction-responsive disulfide-bond-bridged deoxycholic acid−hyaluronic acid to enhance the hydrophobicity of amphiphilic copolymer micelles. They observed that these micelles were degraded in the presence of glutathione and exhibited accelerated hydrophobic drug release.[16] Du et al. synthesized stearate-*g*-dextran copolymers with different grafting degrees of hydrophobic stearate. As the proportion of hydrophobic stearate increased, the loading capacity and encapsulation efficiency increased while their size decreased.[17] The encapsulation efficiency of hydrophobic molecules in an

Received: February 7, 2021
Revised: March 27, 2021
Published: April 9, 2021

https://doi.org/10.1021/acs.biomac.1c00163
Biomacromolecules 2021, 22, 2043−2056

Scheme 1. Structural Design and Application of pH-Responsive Hydrophobic Functional Epoxide Monomer for Amphiphilic Polyether Micelles with High Stability

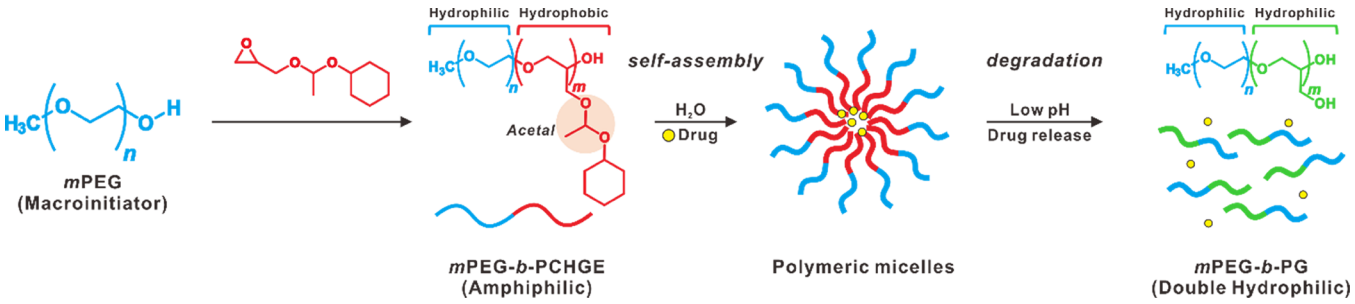

amphiphilic assembly depends on the hydrophobicity.[18] It is thus expected that increasing the hydrophobicity of the core of self-assembled micelles will enhance the interaction with hydrophobic therapeutic agents with enhanced loading capacity and efficiency.

Responsive delivery is another important factor meriting consideration in the design of drug carriers. Polymeric micelles with specific functional groups responsive to various endogenous stimuli such as pH, redox, enzyme or proteins, and nucleic acids have been developed to deliver therapeutic compounds and to control the drug release at target sites.[19] Among diverse stimuli, changes in pH are widely used as a main trigger for inducing drug release.[20] It is well known that the extracellular matrix of tumor cells show a relatively lower pH than normal tissues due to their high preference of glycolysis only at aerobic conditions.[21] Inflammation also causes acidic condition as it promotes the activation of the immune system, which requires acceleration of glycolysis rate.[22] Therefore, pH-responsive micelles with acid-labile linkages such as ketal,[23] acetal,[24] hydrazone,[25,26] and orthoester[27] have been extensively employed.[28]

In our efforts to develop novel functional epoxide monomers for smart drug delivery, we have previously synthesized a series of pH-responsive glycidyl ethers with an acetal group, including tetrahydrofuranyl glycidyl ether (TFGE)[29] and tetrahydropyranyl glycidyl ether (TPGE).[30] While polymeric micelles based on these novel monomers show a pH-responsive controlled release of active therapeutics, it is still highly desirable to develop a monomer with enhanced loading capacity and stability in biological media.

In this context, we herein present a novel hydrophobic epoxide monomer, cyclohexyloxy ethyl glycidyl ether (CHGE), with an acetal group as a pH-responsive cleavable linkage. A series of its homopolymers, poly(cyclohexyloxy ethyl glycidyl ether)s (PCHGE), and block copolymers, poly(ethylene glycol)-*block*-poly(cyclohexyloxy ethyl glycidyl ether)s (*m*PEG-*b*-PCHGE), were synthesized via anionic ring-opening polymerization in a controlled manner. Self-assembled block copolymer micelles of *m*PEG-*b*-PCHGE were formed through strong hydrophobic interactions of CHGE in an aqueous system. Subsequently, the self-assembled micelles were degraded at a low pH due to the pH-responsive acetal bonding of CHGE, and the degradation kinetics could be adjusted by controlling the fraction of the hydrophobic CHGE block (Scheme 1). The CHGE monomer meets the required design principles for drug carriers and addresses the challenges in drug delivery systems to achieve highly tunable polymeric micelles with high loading capacity, high stability, and tailorable release and degradability. Moreover, this novel epoxide monomer system can be extended to synthesize well-defined polymers with superior flexibility and biocompatibility to develop a versatile platform for smart drug delivery systems.

EXPERIMENTAL SECTION

Materials and Reagents. All reagents and solvents were purchased from Sigma-Aldrich, Alfa Aesar, and Tokyo Chemical Industry and used as received unless otherwise noted. Toluene and dichloromethane were dried, degassed using a solvent purification system (Vacuum Atmospheres, USA), and collected for immediate use. Deuterated NMR solvents $CDCl_3$ and D_2O were purchased from Cambridge Isotope Laboratories, Inc. CHGE was used for polymerization after drying over molecular sieves (4 Å).

Characterizations. ^1H NMR (400 MHz) and ^{13}C NMR (100 MHz) spectra were recorded on a Bruker AVANCE III HD NMR spectrometer at room temperature (*ca.* 20 °C). All spectra were acquired in ppm by using D_2O and $CDCl_3$. Gel permeation chromatography (GPC) measurements were performed on an Agilent 1260 Infinity system with two PLgel 5 μm MIXED-D columns at 30 °C; *N*,*N*-dimethylformamide (DMF) was used as the mobile phase with a flow rate of 1.0 mL min^{-1} using a refractive index (RI) detector. Poly(methyl methacrylate) (PMMA) standards were used for calibration to determine the number (M_n)-average and weight (M_w)-average molecular weights and molecular weight distribution (M_w/M_n). Matrix-assisted laser desorption and ionization time-of-flight (MALDI-ToF) mass spectrometry was performed using a Bruker Daltonics LRF20 MALDI-ToF mass spectrometer using 2,5-dihydroxybenzoic acid as the matrix. Differential scanning calorimetry (DSC) was performed on TA Instruments DSC 25 under a nitrogen atmosphere in the temperature range from −80 to 80 °C at a heating rate of 10 °C min^{-1}. Determination of the critical micelle concentration (CMC), encapsulation efficiency with Nile Red, and the release profile of pyrene were obtained using a fluorimeter (RF-6000, Shimadzu). Dynamic light scattering (DLS) measurements were performed using a Zetasizer Nano analyzer (Malvern) equipped with a solid-state laser (λ = 633 nm). The intensity autocorrelation function was measured at an angle of 90 °C. The morphology and diameter of micelles were investigated by atomic force microscopy (AFM; NX10, Park Systems) in a non-contact mode.

Synthesis of the Cyclohexyloxy Ethyl Glycidyl Ether (CHGE) Monomer. A solution of glycidol (15.0 g, 0.202 mol, 1.5 equiv) and cyclohexyl vinyl ether (17.03 g, 0.135 mol, 1.0 equiv) in dichloromethane (200 mL) was added into a round-bottom flask and stirred for 30 min at room temperature. To this solution, *p*-toluenesulfonic acid (0.23 g, 1.35 mmol, 10 equiv) was slowly introduced followed by stirring for 2 h at 0 °C. The solution was stirred for additional 1 h after the addition of saturated $NaHCO_3$ solution. The aqueous phase was extracted with dichloromethane, and the organic layers were extracted with deionized water. The combined organic layers were dried over Na_2SO_4. Then, the solution was concentrated under reduced pressure and purified by flash column chromatography, in which ethyl acetate/hexane (1:9 v/v) was used as the eluent to obtain 22.98 g (85%) of the CHGE monomer as a colorless liquid. This

https://doi.org/10.1021/acs.biomac.1c00163
Biomacromolecules 2021, 22, 2043−2056

Table 1. Characterization Data for All Polymers Synthesized in This Study

polymer code	polymer composition[a]	$M_{n,NMR}$[b] (g mol^{-1})	$M_{n,GPC}$ (g mol^{-1})	M_w/M_n	T_g[e] (°C)	CMC[f] (mg L^{-1})
	$PCHGE_{25}$	5100	4000[c]	1.07[c]	−36.8	
	$PCHGE_{50}$	10,100	2400[c]	1.10[c]	−31.5	
CH7	mPEG$_{144}$-b-$PCHGE_7$	6400	3900[d]	1.09[d]	−35.3	9.49 ± 2.61
CH28	mPEG$_{144}$-b-$PCHGE_{28}$	10,600	3500[d]	1.10[d]	−30.9	2.47 ± 0.34
CH45	mPEG$_{144}$-b-$PCHGE_{45}$	14,000	2700[d]	1.13[d]	−28.6	1.64 ± 0.18
E60	mPEG$_{144}$-b-$PCHGE_{60}$	14,700	14,700	1.11	−59.0	10.3
P37	mPEG$_{144}$-b-$PCHGE_{37}$	11,800	11,600	1.05	−17.0	9.79
F47	mPEG$_{144}$-b-$PCHGE_{47}$	8900	15,300	1.07	−28.0	113.6

[a]Polymerization conversion was over 99%. [b]Determined via ^{1}H NMR spectroscopy. [c]Measured by GPC (THF, RI signal, PMMA standard). [d]Measured by GPC (DMF, RI signal, PMMA standard). [e]T_g was determined by the differential scanning calorimetry (DSC) at a rate of 10 °C min^{-1}. [f]The CMC value was calculated by fluorescence spectroscopy with pyrene as the probe. Polymers E, P, and F have been described in previous studies.[29,30]

monomer was further purified by distillation prior to polymerization. The successful synthesis of the CHGE monomer was confirmed by various characterization techniques, including ^{1}H and ^{13}C NMR, correlation spectroscopy (COSY), heteronuclear single-quantum correlation (HSQC), and electrospray ionization mass spectrometry (ESI-MS) (see Figure 2 for corresponding peak assignments and Figures S1−S4 in the Supporting Information). ^{1}H NMR (400 MHz, $CDCl_3$): δ 4.86 (qd, J = 5.2, 0.6 Hz, 1H), 3.81 (dd, J = 11.3, 3.3 Hz, 1H), 3.69 (dd, J = 11.4, 3.4 Hz, 1H), 3.60−3.49 (m, 1H), 3.41 (dd, J = 11.3, 6.0 Hz, 1H), 3.18−3.09 (m, 1H), 2.83−2.76 (m, 1H), 2.64 (dd, J = 5.1, 2.7 Hz, 1H), 2.60 (dd, J = 5.0, 2.7 Hz, 1H), 1.93−1.80 (m, 2H), 1.79−1.67 (m, 2H), 1.58−1.49 (m, 1H), 1.41−1.11 (m, 8H). ^{13}C NMR (100 MHz, $CDCl_3$): δ 98.14, 98.04, 74.49, 74.34, 65.19, 64.34, 50.94, 50.87, 44.73, 44.60, 33.44, 33.34, 32.65, 32.54, 25.64, 24.39, 24.17, 20.81, 20.58. MS (m/z + Na^+, ESI^+) calcd. for $C_{11}H_{20}O_3$, 223.14; found, 223.13.

Representative Synthesis Procedure for the PCHGE Homopolymer. An amount of 0.125 mL of a solution of t-BuP_4 (0.80 M, 0.10 mmol, 1.0 equiv) in n-hexane was added to a solution of benzyl alcohol (10.4 μL, 0.10 mmol, 1.0 equiv) in toluene under a nitrogen atmosphere. CHGE (1.0 g, 5.0 mmol, 50 equiv) was then added to the solution dropwise by using a syringe pump to initiate polymerization over 6 h. After stirring at room temperature for 24 h, the polymerization was quenched by adding benzoic acid (12.2 mg, 0.10 mmol, 1.0 equiv). The mixture was then passed through an alumina pad using dichloromethane, and the solution was evaporated to dryness to obtain PCHGE (Table 1) (500 mg; yield: 50%). The molecular weight of PCHGE50 was 10,100 g mol^{-1}. This value was calculated from the NMR data shown in Figure 2 by using the following equation: number of repeating units (CHGE) = 50 (integration value of the methine peak, 50H, 4.78 ppm in reference to the methylene peak of benzyl alcohol, 2H, 4.53 ppm); M_n = 200.28 g mol^{-1} (molecular weight of the CHGE monomer) × 50 (number of repeating units) + 108.14 g mol^{-1} (molecular weight of benzyl alcohol) = 10122.14 g mol^{-1}. Considering the error range of NMR integration, we used 10,100 g mol^{-1} as the M_n value of PCHGE50. ^{1}H NMR (400 MHz, $CDCl_3$): δ 4.79 (dd, J = 10.1, 6.4 Hz, 50H), 4.54 (s, 2H), 3.78−3.34 (m, 312H), 1.84 (s, 105H), 1.72 (s, 109H), 1.52 (d, J = 7.1 Hz, 53H), 1.40−1.07 (m, 438H). ^{13}C NMR (100 MHz, $CDCl_3$): δ 98.34, 98.06, 78.96, 73.99, 69.95, 64.77, 64.15, 33.42, 32.51, 25.69, 24.40, 24.16, 20.77 (Figure S5).

Representative Synthesis Procedure for the mPEG-b-PCHGE Block Copolymer. Block copolymers were synthesized using poly(ethylene glycol) methyl ether (mPEG) as a macroinitiator. First, mPEG (1.0 g, 0.20 mmol, 1.0 equiv) was placed in a flask under nitrogen flow. To this flask, 3.0 mL of toluene was added and the mixture was stirred for 30 min at 70 °C. Subsequently, 0.25 mL of t-BuP_4 in n-hexane (0.8 M, 0.20 mmol, 1.0 equiv) was added to the solution. After stirring for 30 min, CHGE (2.0 g, 10.0 mmol, 10 equiv) was added to the solution dropwise by using a syringe pump for 6 h. After stirring at 60 °C for 2 days, the polymerization was terminated by adding benzoic acid (0.02 g, 0.2 mmol). The reaction mixture was passed through a pad of alumina with dichloromethane, and the obtained solution was evaporated to dryness to obtain CH45 (Table 1) (1.98 g; yield: 71%). The molecular weight of CH45 was determined to be 14,000 g mol^{-1} from NMR data (Figure 2) by using the following equation: number of repeating units (CHGE) = 45 (integration value of the methine peak, 45H, 4.80 ppm in reference to the methoxy peak of mPEG, 3H, 3.38 ppm); M_n = 200.28 g mol^{-1} (molecular weight of the CHGE monomer) × 45 (number of repeating units) + 5000 g mol^{-1} (molecular weight of mPEG) = 14,012 g mol^{-1}. Considering the error range of NMR integration, we used 14,000 g mol^{-1} as the M_n value of CH45. ^{1}H NMR (400 MHz, $CDCl_3$) δ 4.85−4.74 (m, 45H), 3.96−3.40 (m, 734H), 3.39 (s, 3H), 1.86 (s, 94H), 1.73 (s, 92H), 1.61−1.47 (m, 44H), 1.42−1.09 (m, 385H). ^{13}C NMR (100 MHz, $CDCl_3$): δ 98.29, 98.03, 78.82, 73.95, 70.54, 69.89, 64.73, 64.21, 33.41, 32.52, 25.66, 24.37, 24.13, 20.80 (Figure S6).

CMC Measurement. A series of polymer solutions in DMF with different concentrations (0.001−1000 mg L^{-1}) were prepared. An amount of 10 μL of a pyrene solution (5.2 mg L^{-1} in DMF) was added to the solution of the mPEG-b-PCHGE block copolymer, and the mixture was stirred for 30 min at room temperature. Subsequently, a 5.0 mL of deionized water was added to the solution at a rate of 0.50 mL min^{-1} by using a syringe pump. After equilibration of the solution overnight, the excitation spectrum of each pyrene-containing polymer micelle solution (with different concentrations) was measured at an emission wavelength of 372 nm by using a fluorimeter in a quartz cell (1 cm × 1 cm). The following parameters were chosen: λ_{em} = 372 nm, λ_{ex} = 280−360 nm, and data interval = 0.5 nm. The ratio between the fluorescence intensities at the wavelengths of 339 and 332 nm (I_{339}/I_{332}) was plotted against the polymer concentration, and the CMC was determined from the inflection point.

Degradation of Micelles. To study the degradation kinetics of polymeric micelles, we prepared two buffer solutions: one at pH 5.0 by using sodium acetate/acetic acid and the other at pH 7.4 by using monobasic/dibasic sodium phosphate. A pyrene-containing polymeric micelle solution was prepared according to the procedure described for the CMC measurement in the preceding paragraph. Subsequently, 0.10 mL of the pyrene-containing micelle solution was slowly added to 0.90 mL of each buffer solution and the changes in the excitation spectra were recorded.

Encapsulation Efficiency of Micelles. The encapsulation efficiency of micelles was determined from the fluorimeter analysis as follows. An amount of 0.10 mL of a Nile Red solution (50 μg mL^{-1} in acetone) was added to a solution of the mPEG-b-PCHGE block copolymer (5 mg) in 0.10 mL of acetone, and the mixture was stirred for 30 min at room temperature. Then, 5.0 mL of deionized water was added slowly to the solution at a rate of 0.50 mL min^{-1} by using a syringe pump. The solution was left to equilibrate overnight, while the lid of the container was left open to allow the acetone to evaporate. After filtration using a 0.45 μm syringe filter for removing unloaded Nile Red, the solution was lyophilized and redissolved in 1.0 mL of

https://doi.org/10.1021/acs.biomac.1c00163
Biomacromolecules 2021, 22, 2043−2056

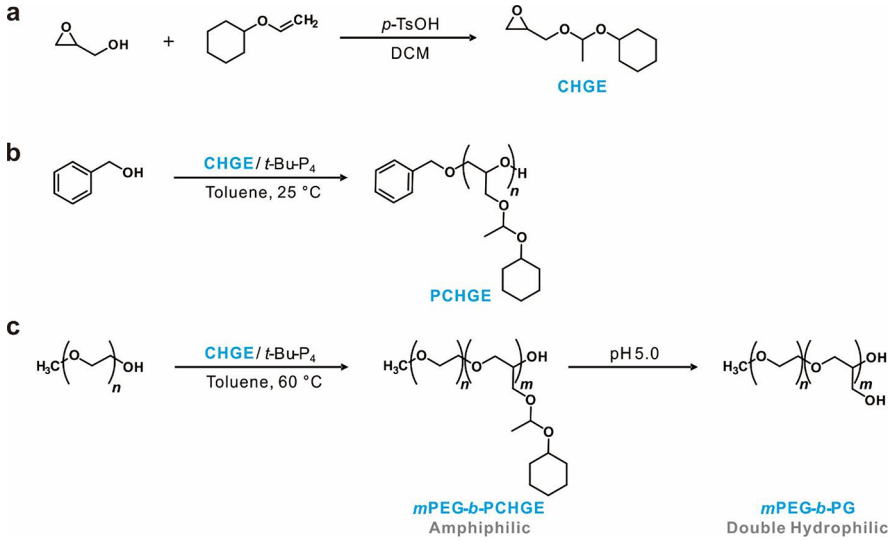

Figure 1. Synthetic scheme for the (a) CHGE monomer, (b) PCHGE homopolymer, and (c) amphiphilic *m*PEG-*b*-PCHGE block copolymer, and the subsequent hydrolysis to double-hydrophilic *m*PEG-*b*-linear polyglycerol (*m*PEG-*b*-PG).

acetone. The amount of Nile Red encapsulated in the micelles was determined by using a fluorimeter in a quartz cell (1 cm × 1 cm) using the following equation:

$$\text{encapsulation efficiency (\%)} = \frac{\text{concentration of Nile Red measured}}{\text{concentration of Nile Red added}} \times 100$$

The following parameters were chosen: λ_{ex} = 480 nm, λ_{em} = 500−800 nm, and data interval = 0.5 nm.

Stability of Micelles in Biological Buffers. A total of 1.0 mL of a solution mixture of DiO and DiI (0.50 mL of each solution; at a concentration of 0.10 mg mL^{-1} in DMF) was added to 0.20 mL of an *m*PEG-*b*-PCHGE solution (25 mg mL^{-1} in DMF) and stirred for 30 min at room temperature. Then, 5.0 mL of deionized water was added slowly to the solution at a rate of 0.50 mL min^{-1} by using a syringe pump. After stirring overnight, the solution was dialyzed against deionized water for 3 days to remove residual DMF. The resulting micelle solution was then filtered through a 0.45 μm syringe filter. A total of 200 μL of the micelle solution was mixed with 800 μL of the respective buffer of phosphate-buffered saline (PBS) and fetal bovine serum (FBS). The stability of different micelles loaded with both DiO and DiI was analyzed for a period of 72 h at room temperature. The excitation was set at 450 nm, and the emission from 460 to 700 nm was detected using a spectrofluorometer.

***In Vitro* Cellular Viability Assay.** SW620 and DU145 cells were grown in RPMI-1640 (with L-glutamine) containing 10% FBS and 1% antibiotic−antimycotic [penicillin 10,000 units mL^{-1}, streptomycin 10,000 μg mL^{-1}, and Fungizone (amphotericin B) 25 μg mL^{-1}]. Furthermore, RAW 264.7 cells were grown in Dulbecco's modified Eagle medium (high glucose) containing 10% FBS and 1% antibiotic−antimycotic. The cells were cultured in a humidified incubator at 37 °C with 5% CO_2. Cell viability was quantified by the MTT assay [MTT denotes 3-(4,5-dimethyl-2-thiazolyl)-2,5-diphenyl-2*H*-tetrazolium bromide]. The cells were seeded in a 96-well plate at a concentration of 1.5 × 10^5 cells per milliliter and incubated overnight. Subsequently, micelles of different concentrations (0, 25, 50, 100, and 200 μg mL^{-1}) were added to the cell culture media, and the cells were incubated for an additional 24 h at 37 °C with 5% CO_2 in the dark. Next, 100 μL of an MTT solution (5 mg mL^{-1} PBS, pH 7.4) was added to each well, and the cells were further incubated for 3 h. The old medium containing unreacted MTT was removed carefully, and formazan produced by living cells was dissolved in DMSO at room temperature. The absorbance at 570 nm was measured using a microplate reader (BioTek Instruments, Winooski, VT).

Cellular Uptake and Endosomal Escape of Micelles. SW620 cells (2 × 10^6) were seeded in a glass-bottom dish and incubated for 24 h. After incubation, the cells were then treated with Nile Red-loaded CH28 micelles for predetermined time periods and washed with fresh PBS three times. Cells were also treated with LysoTracker for 30 min to stain the endosomes and lysosomes. Fluorescence images of the cells were acquired using a confocal laser scanning microscope (Carl Zeiss, Germany).

***In Vivo* Mouse Xenograft Assay with Paclitaxel-Loaded Micelles.** SW620 cells (2 × 10^6) were directly injected into the flank of 6 week-old mice, which were randomly divided into five groups. When the average tumor volume reached approximately 50 mm^3, the mice were administered an intravenous injection of paclitaxel (PTX) (2 mg kg^{-1}), empty CH28 micelles (20 mg kg^{-1}), and PTX-loaded CH28 micelles (10 or 20 mg kg^{-1}) every 3 days. The tumor volume and body weight were observed for 25 days. The tumor volume was calculated as (width^2 × length)/2. For fluorescence imaging, IR780-encapsulated CH28 micelles were intravenously injected into the tail vein at a dose of 10 mg kg^{-1}. Fluorescence images were acquired using FOBI (NeoScience, Korea) with a near-infrared (NIR) channel.

***In Vivo* Biocompatibility of Micelles.** CH28 micelles were intravenously injected into healthy mice (approximately 20 g) at a dose of 20 mg/kg on each day (1, 3, and 5 days). After euthanization, whole blood and major organs (liver, lung, kidney, heart, and spleen) were collected on day 7. The level of serum alanine transaminase (ALT) was measured using an ALT kit (Asan Pharma, Korea). Organs embedded in a paraffin block were sectioned for histological examination. Tissue sections were stained with hematoxylin and eosin and observed under an optical microscope.

Details of Computational Calculations. All calculations, including those for each acetal molecule containing 25 water molecules and an additional proton, were performed with the B3LYP/6-31+G* level of theory, which was implemented in the TeraChem program. The polarizable continuum model for water was used for considering the solvent's effects.

RESULTS AND DISCUSSION

Synthesis of CHGE Monomer and Polymerization. A pH-responsive hydrophobic monomer CHGE was synthesized through a one-step coupling reaction between glycidol and cyclohexyl vinyl ether (Figure 1a). The synthesized CHGE monomer was purified by column chromatography and fractional distillation to give a typical isolated yield of 85%. The chemical structure of CHGE was successfully verified

https://doi.org/10.1021/acs.biomac.1c00163
Biomacromolecules 2021, 22, 2043−2056

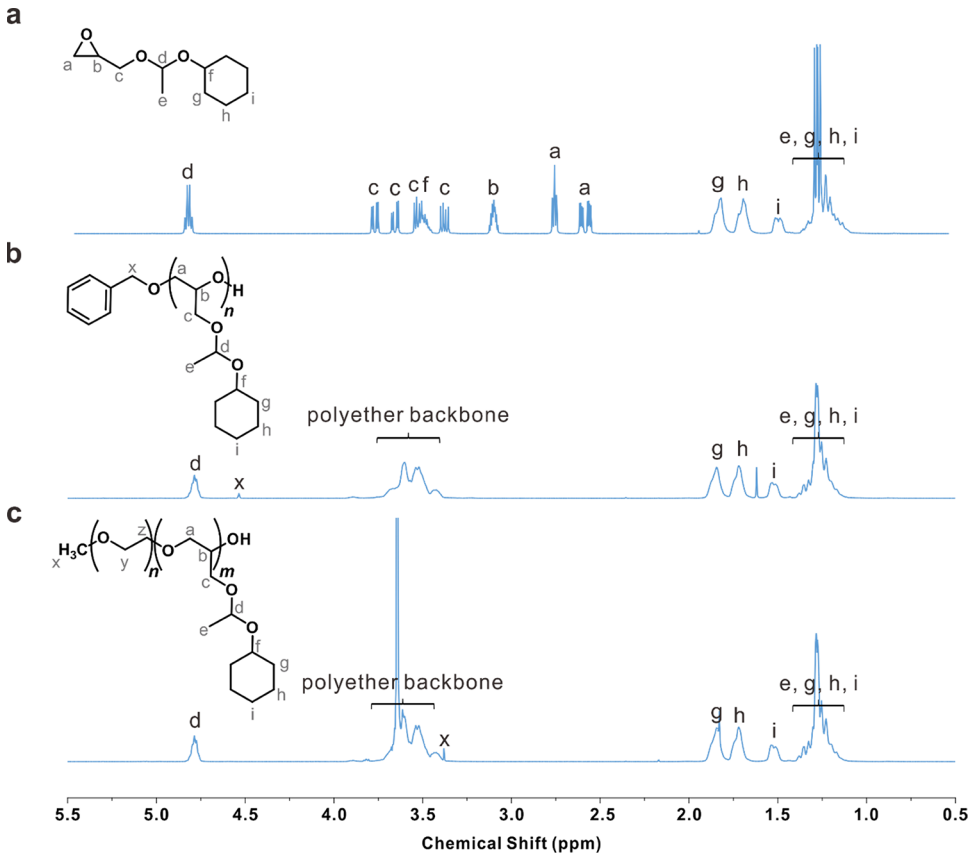

Figure 2. Representative ^{1}H NMR spectra of the (a) CHGE monomer, (b) PCHGE$_{50}$ homopolymer, and (c) *m*PEG-*b*-PCHGE block copolymer (CH45 in Table 1). All spectra were collected in $CDCl_3$.

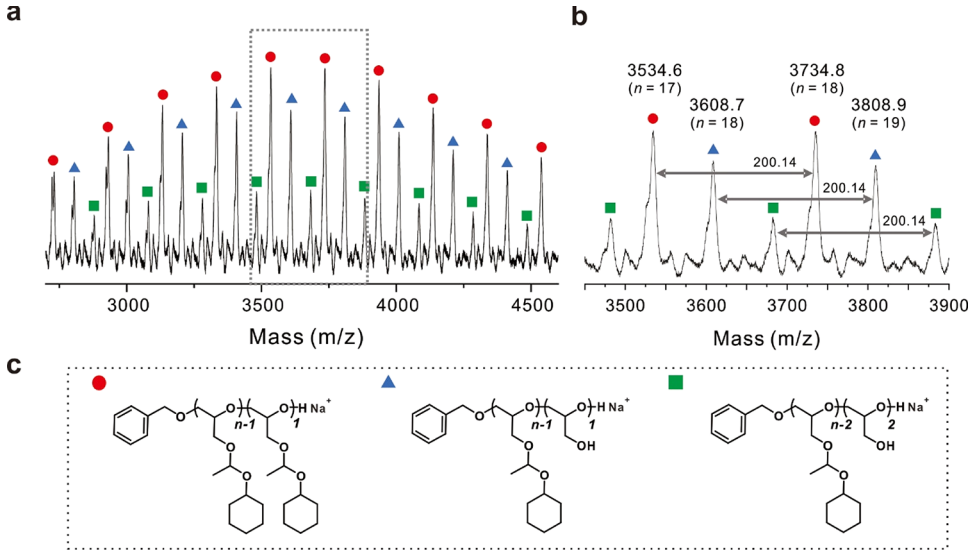

Figure 3. (a) Representative MALDI-ToF mass spectrum of the PCHGE$_{50}$ homopolymer for the mass range 2750−4500 Da and (b) individual peak assignments in the selected region in panel (a). (c) Chemical structures of polymers (red circles) and partially degraded polymeric fragments (blue triangles and green squares) during the measurement.

using various NMR spectroscopic techniques, including ^{1}H, ^{13}C, correlation spectroscopy (COSY), heteronuclear single-quantum correlation (HSQC), and electrospray ionization mass spectrometry (ESI-MS) (Figure 2a and Figures S1−S4 in the Supporting Information).

After the successful investigation of the CHGE monomer, anionic ring-opening polymerization was performed by using benzyl alcohol as an initiator and the phosphazene base *t*-BuP_4 as an organic superbase at room temperature (*ca.* 25 °C) (Figure 1b). The highly basic organic superbase *t*-BuP_4 was used as it facilitates the controlled polymerization of CHGE monomer under mild conditions.[31] The synthesized PCHGE homopolymers were characterized by ^{1}H NMR, ^{13}C NMR, GPC, DSC, and MALDI-ToF mass spectrometry (Figures 2b

https://doi.org/10.1021/acs.biomac.1c00163
Biomacromolecules 2021, 22, 2043−2056

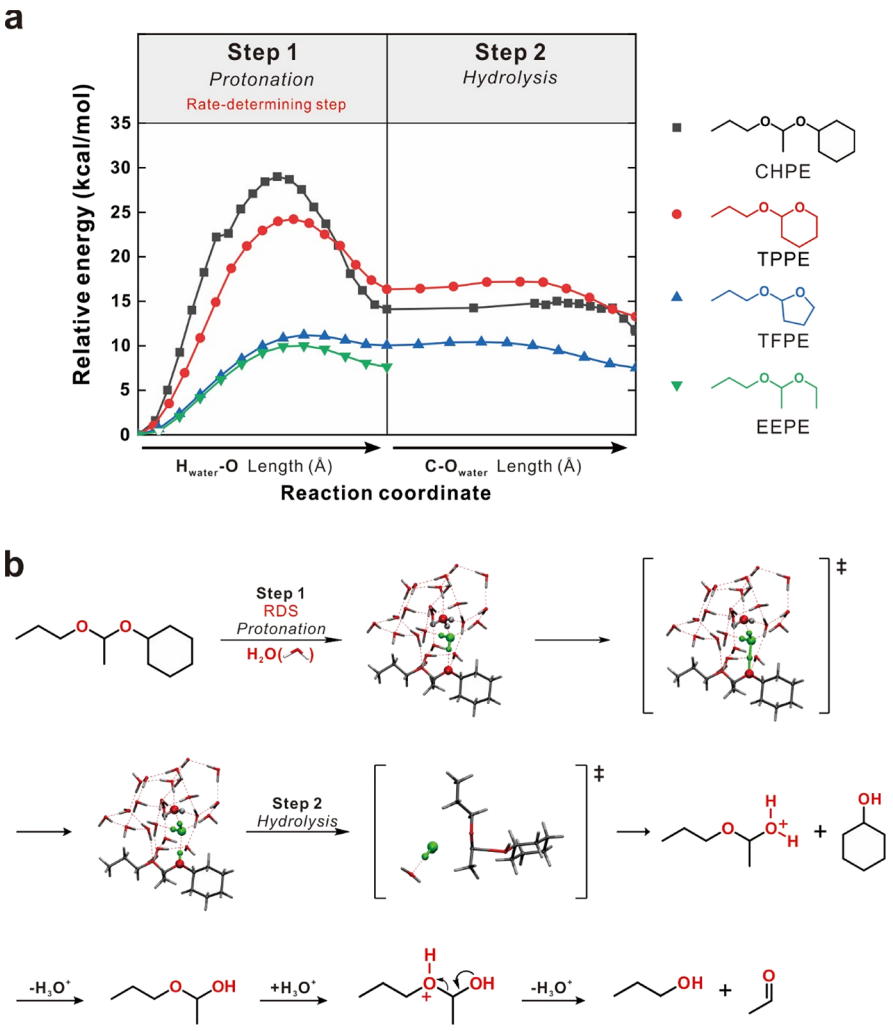

Figure 4. (a) Energy diagram of various model acetal compounds in the course of hydrolysis and (b) proposed hydrolysis mechanisms for CHPE with the hydration shell. The green molecule is the water molecule involved in the hydrolysis of CHPE.

and 3 and Figures S5 and S7). The molecular weights of the homopolymers were controlled through the monomer-to-initiator ratio, which yielded the molecular weights (*i.e.*, $M_{n,NMR}$) of PCHGEs in the range of 5000−10,000 g/mol with a narrow dispersity ($Đ$ = 1.07−1.10).

As shown in Figure 2b, the ^{1}H NMR spectra indicated that the conversion of the monomer to polymer was accompanied by the disappearance of the epoxide peaks (*a* and *b*) in the monomer at 2.60, 2.80, and 3.15 ppm (Figure 2a). Moreover, the other peaks in the PCHGE homopolymer were clearly assigned, including those of the benzylic protons (x; 4.52−4.55 ppm), polyether backbone protons (a, b, and c; 3.40−3.75 ppm), methine protons (d; 4.75−4.85 ppm), and methyl and cyclohexyloxy protons (e, g, h, and i; 1.10−1.90 ppm). The theoretical number-average molecular weight ($M_{n,NMR}$) was calculated as the ratio of the integral of benzylic protons to that of methine proton in the ^{1}H NMR spectra.

In the next step, a block copolymer consisting of a hydrophilic PEG block and a hydrophobic PCHGE block was prepared to produce a series of amphiphilic block copolymers (*m*PEG-*b*-PCHGE) with varying degrees of hydrophobic PCHGE blocks (Table 1). As shown in Figure 2c, the ^{1}H NMR spectra of the block copolymer clearly showed each characteristic peak of the different structures: the methyl protons of the *m*PEG macroinitiator (x; 3.38 ppm), methine proton (d; 4.75−4.80 ppm), polyether backbone protons (y, z; 3.40−3.75 ppm), and methyl and cyclohexyloxy protons (e, g, h, and i; 1.10−1.90 ppm). The degree of polymerization (DP) of the amphiphilic block copolymer was determined by the ratio of the methine peak (g; 4.75−4.80 ppm) of CHGE to the methyl peak (3.38 ppm) of *m*PEG. GPC results of the block copolymer also showed monomodal distributions with narrow dispersity ($Đ$ < 1.13) in all entries (Figure S8). It is worth noting that the $M_{n,GPC}$ values tend to be considerably lower than the $M_{n,NMR}$ values, as shown in Table 1. This observation could be attributed to the high hydrophobicity of the CHGE monomer in the homopolymers and block copolymers, which in turn led to the difference in their hydrodynamic volumes in the solvent. With increasing the fraction of the CHGE block, this difference in their molecular weights becomes more pronounced as indicated in both homopolymers and block copolymers. To confirm the pH-responsive nature of the synthesized block copolymer, ^{1}H NMR analysis was performed after the CH45 polymer was treated in acidic conditions. As a result of deprotection in acidic conditions, all of the peaks corresponding to the side chain of CHGE disappeared (Figure S9).

https://doi.org/10.1021/acs.biomac.1c00163
Biomacromolecules 2021, 22, 2043−2056

After confirming the successful synthesis of the PCHGE homopolymers via NMR and GPC, MALDI-ToF spectrometry was performed to determine the successful incorporation of CHGE into the PCHGE homopolymer. In the MALDI-ToF spectrum, the molecular weight of 3734.8 g mol^{-1} can be assigned to a homopolymer comprising the benzyl alcohol initiator (108.06 g mol^{-1}) and 18 monomers (200.14 g mol^{-1}) with Na^+ as the counterion. Interestingly, two types of minor peaks are also observed, which resulted from the partial degradation of the cyclohexyloxy group during the measurement. Above all, the spacing of major and minor signals corresponded to the molecular weight of the functional CHGE monomer, indicating successful polymerization.

DSC analysis provided the glass transition temperatures (T_g) of the PCHGE homopolymers and amphiphilic *m*PEG-*b*-PCHGE block copolymers (Table 1 and Figure S7 and S8). Interestingly, the T_g value increased from −36.8 to −31.5 °C as the DP of CHGE in the PCHGE homopolymers increased. From these results, we postulate that the higher T_g values could be attributed to the increased chair-to-chair stacking of the cyclohexyl groups of CHGE. Similarly, with an increase in the DP of CHGE in the amphiphilic block copolymer, the T_g of the polymer increased from −35 °C (CH7) to −28 °C (CH45). Interestingly, the T_g of the *m*PEG-*b*-PCHGE polymers are similar to that of block copolymers based on TFGE monomers but lower than that of TPGE-based block copolymers. While the packing of the cyclic pendant structures is similar in all these copolymers, it can be postulated that the relatively linear structure of CHGE led to a lower T_g value compared with the TPGE-based block copolymers.

Before the examination of the self-assembly behavior of the amphiphilic block copolymers prepared in this study, we investigated the hydrolysis kinetics of the CHGE monomer through quantum mechanical calculations based on density functional theory (Figure 4). Quantum mechanical analysis provides crucial information of the kinetic energy barrier and the structure and relative energy of intermediates involved during the hydrolysis of functional monomers. Considering the structure of the side chains formed after the polymerization of the CHGE monomer, we synthesized a new model compound, cyclohexyloxy propyl ether (CHPE) (see the Experimental Section for details). Furthermore, the hydrolysis kinetics of the CHGE monomer were compared with that of a series of other types of monomers with acetal groups reported in our previous studies, such as tetrahydropyranyl propyl ether (TPPE), tetrahydrofuranyl propyl ether (TFPE), and ethoxyethyl propyl ether (EEPE).[29]

In the first step, 25 explicit water molecules (25 H_2O) and an additional proton were considered in the calculation of energy barriers during protonation. The optimized structure of the model compound with the lowest-energy structures was obtained, including the transition-state structures before and after protonation. Interestingly, protonation was performed for the outer shell made of the water molecules in CHPE, indicating the high hydrophobicity of the model compound. Subsequently, the reaction energy barrier (ΔE) was calculated for constrained optimization by considering it to depend on the distance between oxygen and proton in the CHPE structure. The reactive energy profiles showed the protonation of model acetal compounds according to the O−H bond length. It is noteworthy that the CHPE (29.0 kcal mol^{-1}) showed a higher energy barrier (ΔE) for protonation than those of the other monomers, including TPPE (24.2 kcal mol^{-1}), TFPE (11.2 kcal mol^{-1}), and EEPE (10.0 kcal mol^{-1}), indicating that CHPE had the highest hydrophobicity compared to other acetal model compounds. In parallel, the hydrophobicity of each monomer was also estimated using the partition coefficient (log *P*) with the computational model ALOGPS 2.1. The calculated log *P* values were 2.93 (CHPE), 1.72 (TPPE), and 1.31 (TFPE),[32] which supported the observed trends in the reactive energy profiles.

Generally, the overall hydrolysis of acetal linkages comprises two steps: (1) a protonation step and (2) a bond cleavage step. For CHPE, the rate-determining step in the overall hydrolysis was found to be a protonation reaction with a maximum reaction energy barrier value of 29.0 kcal mol^{-1}. We then calculated the reaction energy barrier and transition state in the hydrolysis step of the protonated CHPE compound (*i.e.*, H^+-CHPE; Figure 4b) with two explicit water molecules in the hydrolysis of the protonated CHPE compound for an activation energy barrier of approximately 1.0 kcal mol^{-1}. This process was also observed for the ring opening of H^+-TPPE and H^+-TFPE with a single transition state involving significantly lower energy barriers (0.83 and 0.37 kcal mol^{-1}, respectively) compared with the protonation step. In the case of H^+-EEPE, no activation energy barrier was observed for C−O bond breaking, indicating that the concurrent hydrolysis was followed by the protonation step.

Motivated by the computational analysis of the model compounds, we performed the hydrolysis of the CHPE model compound by *in situ* ^1H NMR spectroscopy under acidic conditions with a sodium acetate-d_3/acetic acid-d_4 buffer at pH 5.0. However, the limited solubility of the CHPE monomer in an aqueous buffer prevented the monitoring of hydrolysis, unlike other model acetal compounds. In concert with the computational calculation results, the high hydrophobicity of the CHPE model compound supports the prolonged hydrolysis of the acetal group in CHPE.

Self-Assembly Behavior of *m*PEG-*b*-PCHGE Amphiphilic Block Copolymers. The CMC value of self-assembled polymeric micelles is a crucial parameter to predict the stability of the micelles.[33,34] The CMC value of the amphiphilic polymer was determined using pyrene as a fluorescent probe. Specifically, when pyrene is encapsulated within the hydrophobic core of micelle, the (0,0) band in the pyrene excitation spectra is red-shifted from 332 nm (water) to around 339 nm.[35,36] By taking advantage of this feature, pyrene has been widely used for determination of CMC in the literature[37,38] including our previous contributions.[29,30] For example, the I_{339}/I_{332} (intensity ratio of 339 nm over 332 nm) was plotted according to the different concentrations of each polymer. A clear crossover point was observed in all polymers, and the obtained CMC values of the amphiphilic polymers were 9.49 ± 2.61 (CH7), 2.47 ± 0.34 (CH28), and 1.64 ± 0.18 mg L^{-1} (CH45) (Figure S10). The CMC values of the amphiphilic polymer decreased with an increase in the polymerization degree of hydrophobic blocks. These CMC values were lower than those of other polymers prepared from acetal-based functional epoxide monomers, including E60 (10.3 mg L^{-1}), P37 (9.79 mg L^{-1}), and F47 (113.6 mg L^{-1}), prepared from ethoxyethyl glycidyl ether (EEGE), TPGE, and TFGE monomers, respectively.[29,30] This result can be correlated to the enhanced hydrophobicity of the CHGE monomers in the hydrophobic core of the micelles.

After confirming micelle formation, we also determined the size and shape of the micelles by dynamic light scattering

https://doi.org/10.1021/acs.biomac.1c00163
Biomacromolecules 2021, 22, 2043−2056

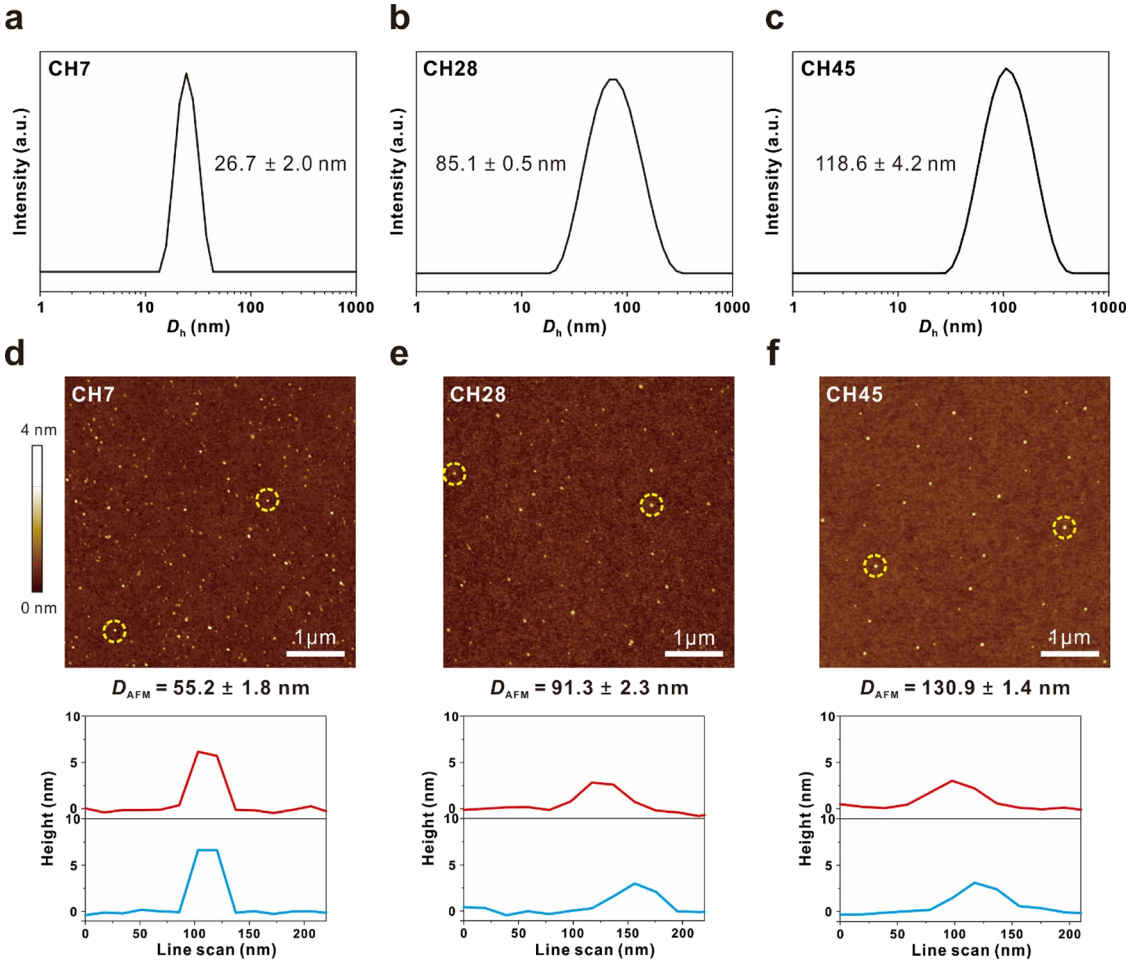

Figure 5. (a–c) Distribution of the intensity-averaged hydrodynamic diameter (D_h) of CH7, CH28, and CH45 micelles measured by DLS. (d–f) Height-mode AFM images of CH7, CH28, and CH45 micelles with the corresponding line scan profiles.

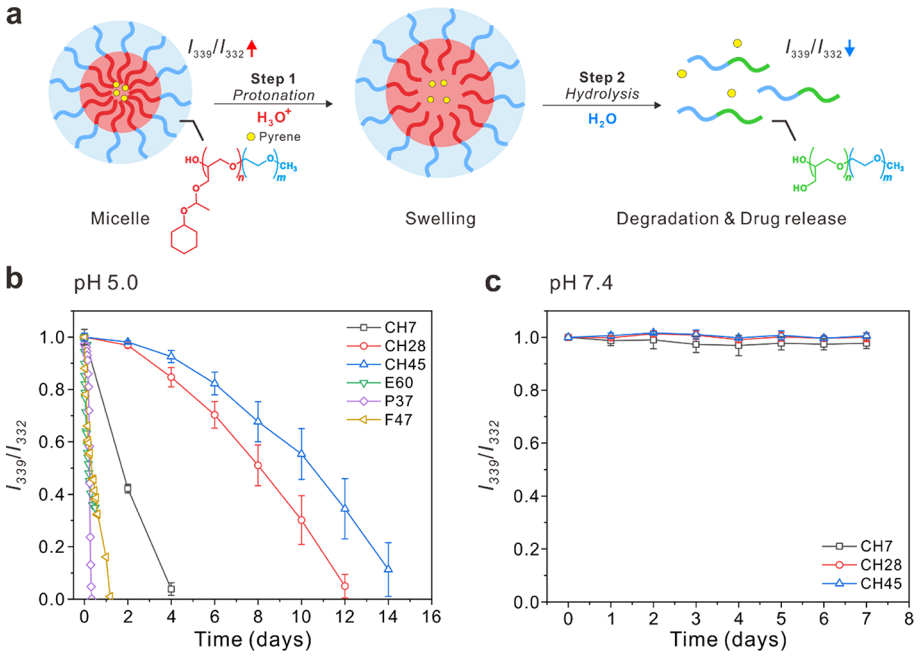

Figure 6. (a) Schematic representation and the corresponding chemical changes in drug-release profiles based on the pyrene fluorescence method. (b, c) Drug-release kinetics of pyrene-loaded micelles at (b) pH 5.0 and (c) pH 7.4 at 37 °C. The data for E60, P37, and F47 were collected from our previous reports.[29,30]

https://doi.org/10.1021/acs.biomac.1c00163
Biomacromolecules 2021, 22, 2043−2056

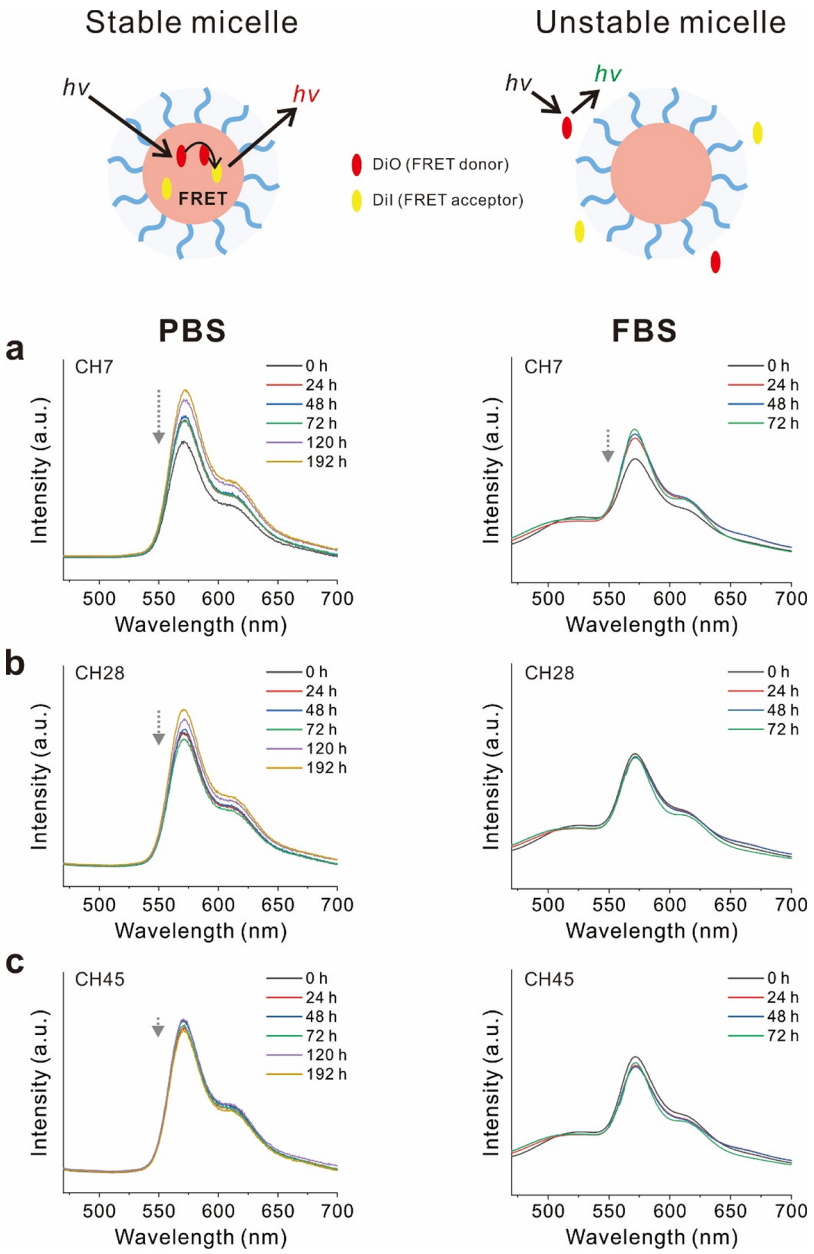

Figure 7. FRET-based stability analysis of various micelles under different biological conditions using fluorescence emission spectra (λ_{ex} = 450 nm) in (left panel) PBS and (right panel) FBS. (a) CH7, (b) CH28, and (c) CH45 micelles. The emission peak of DiO (FRET-donor) is observed at 510 nm, and that of DiI (FRET-acceptor) occurs at 560 nm.

(DLS) and atomic force microscopy (AFM). The concentration of all polymers used in the DLS measurement was above the CMC values (1 mg mL^{-1}). The hydrodynamic diameter (D_h) of each micelle measured by DLS was 26.7 ± 2.0 (CH7), 85.1 ± 0.5 (CH28), and 118.6 ± 4.2 nm (CH45) (Figure 5a–c), and the diameter increased with the number of CHGE monomers. We postulate that steric hindrance exists in the hydrophobic core of micelles following an increase in the number of bulky hydrophobic CHGE units, which results in the increased size of the micelle. Moreover, the morphology of micelles was analyzed with AFM. As shown in Figure 5d–f, the AFM images showed a spherical shape of the micelle with a narrow distribution of the diameter (CH7: D_{AFM} = 55.2 ± 1.8 nm; CH28: D_{AFM} = 91.3 ± 2.3 nm; and CH45: D_{AFM} = 130.9 ± 1.4 nm), in good agreement with the DLS results.

As an important factor of drug delivery carriers, the encapsulation efficiency of the micelles was investigated using Nile Red as a model hydrophobic dye within the hydrophobic core of the micelles. The loading efficiencies of Nile Red in the micelle cores were determined to be 20.4% (CH7), 57.6% (CH28), and 61.5% (CH45) (Figures S11 and S12). These were higher than those for other E, P, and F series micelles, which had values such as 10.9% (E60), 16.6% (P37), and 9.8% (F47).[29,30] Overall, the introduction of the highly hydrophobic and bulky CHGE monomer in the polymer provided driving force for the formation of micelles with excellent loading efficiency.

Degradation Kinetics and Encapsulation Stability of Polymeric Micelles. Although polymeric micelles are promising drug delivery carriers, their stability continues to pose a challenge in biological applications.[39,40] In particular,

https://doi.org/10.1021/acs.biomac.1c00163
Biomacromolecules 2021, 22, 2043–2056

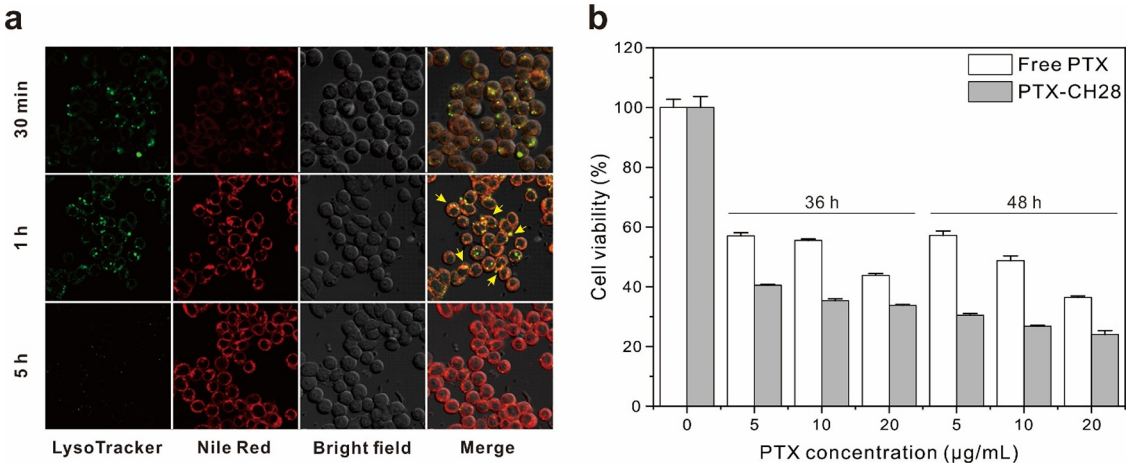

Figure 8. (a) Cellular uptake and endosomal escape of CH28 micelles. Arrows indicate the co-localization of Nile Red-loaded CH28 micelles and green LysoTracker in endosomes and lysosomes. (b) *In vitro* cell cytotoxicity assay of CH28 micelles determined by the MTT assay using SW620 cells. Free PTX (empty bars) and PTX-loaded CH28 micelles (filled bars) incubated for 36 and 48 h.

among the various biological substances that can be encountered during circulation in the blood stream, encapsulation of hydrophobic drugs is affected by various proteins present in the blood. Therefore, the stability of the micelles was investigated in various environments, including those with different pH conditions and different biological buffers (Figures 6 and 7).

First, the stability of pyrene-containing micelles was monitored for changes in the I_{339}/I_{332} ratio in acidic (pH 5.0) and normal (pH 7.4) environments at 37 °C (Figure 6b,c). We investigated the degradation of micelles by monitoring changes in the I_{339}/I_{332} ratio in the excitation spectra of pyrene. The intensity of I_{339}/I_{332} in all micelles (CH7−CH45) remained unchanged, indicating that all micelles were stable at pH 7.4. However, in the acidic environment with pH 5.0, a change in the CHGE moieties of the micelles to hydrophilic linear polyglycerol (PG) as a result of hydrolysis and degradation was observed. As the micelles reacted at a low pH, the intensities of all micelles decreased over time as the encapsulated pyrene in the core was released; the intensity of CH7 decreased most noticeably. Interestingly, the release rate of pyrene was lower with an increase in the number of units of CHGE monomers in the micelles. For example, CH7 was degraded most rapidly (in 4 days) and released the largest amount of pyrene. By contrast, CH28 and CH45 were completely degraded in 12 and 14 days, respectively. These results are in consistent with the CMC values of CH series micelles and suggest that the release kinetics can be highly controlled, which allows to tailor the burst release to sustained release through appropriate selection of the hydrophobicity of the micelle cores.

Next, we investigated the stability of the micelles in various biological environments, phosphate-buffered saline (PBS) and fetal bovine serum (FBS). In a previous study, a fluorescence resonance energy transfer (FRET)-based method was employed to determine the stability of micelles in biological environments.[8] The stability of a micelle was analyzed by loading the FRET pair of DiO (FRET-donor) and DiI (FRET-acceptor) into the hydrophobic core of the micelle. If the micelle is stable under harsh conditions, efficient energy transfer from DiO to DiI occurs because the FRET pair is located close in the core, which results in a strong emission near 560 nm.[41] However, if the micelle is unstable, the FRET pair is freely located and there is no energy transfer between DiO and DiI; therefore, only the strong emission of DiO at 510 nm would appear.

As shown in Figure 7, the CH7, CH28, and CH45 micelles showed strong emissions only at approximately 550 nm in PBS for 192 h, and no peak was observed at 510 nm. As mentioned, this result was obtained because of the efficient energy transfer owing to the proximity of DiO and DiI in the core of the micelle, which indicated excellent micelle stability in the PBS. Interestingly, peak variation was rarely observed in the CH45 micelle during the entire measurement duration; however, in the CH28 and CH7 micelles, a larger peak variation was observed after 120 h. From these results, we conclude that the higher the number of hydrophobic units, the denser the DiO and DiI in the core; therefore, the core of the micelle was more stable and no peak variation was observed.

We measured the stability of the micelles in the FBS only up to 72 h due to the formation of protein and lipid aggregates present in the FBS. A strong emission at 550 nm was observed in all the micelles for 72 h, and no peak change at 510 nm was observed. As with the PBS data, the peak variation was observed only in CH7, not in CH28 and CH45. These results indicate that all micelles were unaffected by the proteins in the serum and could safely hold the payload in the core. Taken together, we confirmed that the micelles exhibited excellent stability in the biological environments and degraded in response to a low acidic pH.

Internalization and Endosomal Escape of CH28 Micelles and Anticancer Activity. Finally, to evaluate the potential of the micelles for application in drug delivery systems, we investigated the cellular uptake, endosomal escape, and *in vitro* cytotoxicity of the micelles by the MTT assay. Once taken up by cells, drug delivery systems must overcome the endosomal entrapment followed by the release of payloads in the cytosol of cells for the full realization of the therapeutic activity.[42] Cellular uptake and endosomal escape of CH28 micelles were analyzed by confocal fluorescence microscopy using Nile Red-loaded CH28 micelles and green LysoTracker (Figure 8a). The SW620 cells display strong green fluorescence only in acidic environments such as endosome and lysosome. Starting from 30 min after incubation, Nile Red-loaded CH28 micelles were taken up by cells, as evidenced by weak red fluorescence on the cell membrane. After incubation

https://doi.org/10.1021/acs.biomac.1c00163
Biomacromolecules 2021, 22, 2043−2056

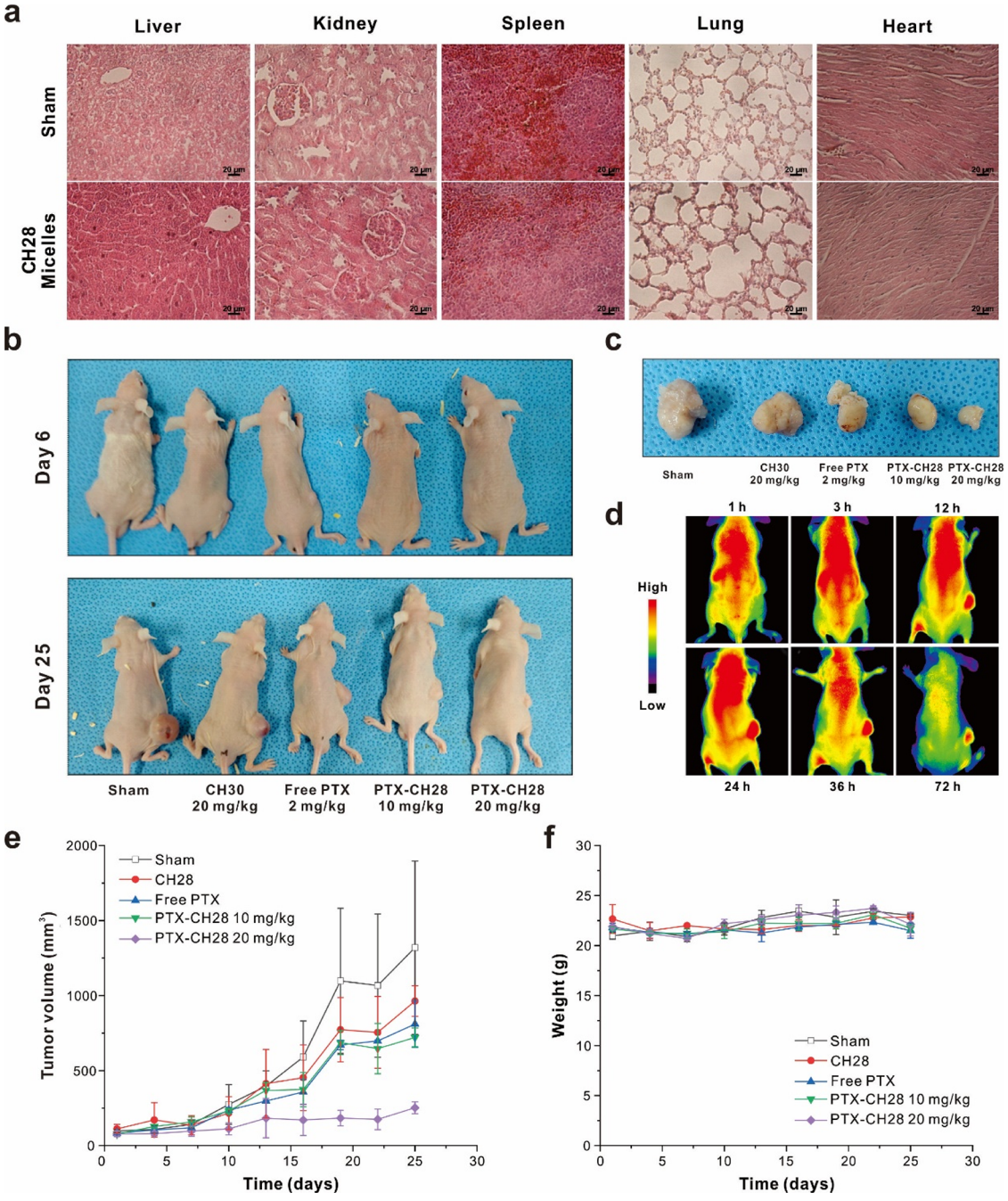

Figure 9. Evaluation of CH28 micelles as a drug carrier *in vivo*. (a) Histological examination of major organs of a mouse upon treatment of CH28 micelles. (b, c) Representative images of tumor-bearing mice during treatment with PTX, free micelles, and PTX-loaded micelles after day 6 and day 25 along with (c) images of collected tumor volume of respective mouse. (d) Representative fluorescence imaging of tumor-bearing mice at 3 h post-injection of IR780-encapsulated CH28 micelles. (e) Changes in tumor volumes and (f) body weight changes of mice under different treatment conditions. Values are reported with a mean with standard deviation (n = 4). See the Experimental Section for details.

for 1 h, yellow fluorescence was observed in cells due to the co-localization of the red signal from Nile Red-loaded CH28 micelles and the green signal from endosomes and lysosomes labeled with LysoTracker, indicating the entrapment of CH28 micelles in endosomes and/or lysosomes.[42] Eventually, the red fluorescence spread to the cytosol after 5 h of incubation and, most notably, the green fluorescence significantly decreased due to the loss of fluorescence of LysoTracker upon release in the cytosol with neutral pH. These observations support the endosomal escape of Nile Red-loaded CH28 micelles induced by the influx of protons and osmotic pressure buildup in acidic endosomes, thus triggering the degradation of CH28 micelles.[43,44]

To investigate the cell cytotoxicity assay, the SW620 cells and RAW cells were treated with each micelle, and their cellular viability was evaluated using the MTT assay (Figure S13). After the micelle solution was treated with varying cell concentrations, the cell viability was nearly 100% in the CH7, CH28, and CH45 micelles, even at a high concentration of 200 μg mL^{-1}, suggesting their suitability as a drug delivery carrier.

In addition, we demonstrated the therapeutic efficacy of micelles loaded with paclitaxel (PTX), a poorly water-soluble

https://doi.org/10.1021/acs.biomac.1c00163
Biomacromolecules 2021, 22, 2043−2056

anticancer drug. In particular, the CH28 micelle was chosen as a representative example owing to its high drug-loading capability and appropriate time scale of degradation. As shown in Figure 8b, the cell cytotoxicity increased with the drug concentration, indicating the effective delivery of PTX to the cancer cells. Upon incubation for a longer time, more active release of PTX enhanced the cytotoxicity. It is also noteworthy that the cytotoxicity was higher for PTX-loaded CH28 than that of free PTX, indicating the higher therapeutic efficacy of PTX-loaded CH28 micelles possibly due to the enhanced bioavailability of PTX within the cells. Through the endocytosis process followed by the pH-responsive degradation of the micelles, the PTX loaded within the micelles are released in a controllable manner.

Anticancer Activity of Drug-Loaded Polymeric Micelles. After confirming the successful internalization and endosomal escape of micelles and their excellent efficiency as a drug delivery carrier, we performed more investigations in detail through *in vivo* mouse experiments. Specifically, healthy mice were intravenously administrated with CH28 micelles at a dose of 20 mg/kg every other day, and the blood and major organs were collected on day 7 for analysis. The level of serum alanine transaminase (ALT) was measured to determine whether CH28 micelles induce liver damage. There was no significant difference in the level of serum ALT between the sham and CH28 micelle-treated mice, indicating that CH28 micelles induce no damage to hepatocytes (Figure S14).[45] Histological examination was also performed using tissues of major organs (Figure 9a). The tissues showed no significant histological evidence of accumulated toxicity. These findings suggest that CH28 micelles have excellent safety profiles at a therapeutic dose *in vivo*.

Furthermore, a mouse xenograft model was used to evaluate the efficacy of CH28 micelles as a drug carrier loaded with PTX. PTX was loaded in CH28 micelles during self-assembly, with approximately 8 wt % loading content. When the tumor volume reached 50 mm^3, mice were treated with free PTX (2 mg kg^{-1}), empty CH28 micelles, and PTX-loaded CH28 micelles (10 or 20 mg kg^{-1}). Tumor volumes and the body weight were observed for 30 days post-tumor inoculation. Free PTX significantly inhibited tumor growth compared with the untreated control group. However, PTX-loaded CH28 micelles exhibited remarkable suppression of tumor growth, showing significantly higher therapeutic effects than free PTX (Figure 9a,b). No significant body weight change was observed during the treatment, indicating minimal toxicity of each treatment (Figure 9c). Fluorescence imaging was also performed to investigate the biodistribution of CH28 micelles that encapsulated fluorescent IR780. As shown in Figure 9d, strong fluorescence was observed in tumors preferentially 3 h after injection, and the fluorescence signal in tumors lasted for more than 72 h. The passive, but preferential, tumor accumulation of CH28 micelles could be explained by their excellent colloidal stability and enhanced penetration and retention effects in leaky tumor vasculature.[46,47] The superior therapeutic effects of PTX-loaded CH28 micelles over free PTX can also be accounted by the capability of the CH28 micelles to target tumor passively.

CONCLUSIONS

In summary, we present the design and synthesis of a novel hydrophobic epoxide monomer, CHGE, to obtain a pH-responsive hydrophobic block in drug delivery micelles with excellent stability and high loading efficiency. The organic superbase promoted anionic ring-opening polymerization, which yielded well-defined PCHGE homopolymers and amphiphilic block copolymers of *m*PEG-*b*-PCHGE with controlled molecular weights and narrow dispersity. The polymeric micelles prepared from a series of *m*PEG-*b*-PCHGE polymers demonstrated excellent stability, encapsulation efficiency, and highly controllable release kinetics. Compared to existing acetal-based monomers developed thus far, the polymeric micelles based on the CHGE monomer exhibited considerably lower CMC values, higher loading efficiency, and enhanced stability, which could be attributed to the increased hydrophobicity that retarded the hydrolysis rate of the hydrophobic block. Finally, the high biocompatibility of the micelles clearly demonstrates the potential of *m*PEG-*b*-PCHGE as potential drug delivery carriers. The preferential cellular uptake and therapeutic efficacy *in vivo* further confirmed the suitability of amphiphilic block copolymer micelles for use as a smart drug delivery carrier. We anticipate that the new class of functional epoxide monomer and polymers developed in this study will contribute to the development of functional polyethers and emerge as promising candidates for biomedical applications.

ASSOCIATED CONTENT

Supporting Information

The Supporting Information is available free of charge at https://pubs.acs.org/doi/10.1021/acs.biomac.1c00163.

NMR, ESI-MS, GPC, DSC, CMC, DLS, AFM, encapsulation efficiency, and MTT assay of micelles (PDF)

AUTHOR INFORMATION

Corresponding Author

Byeong-Su Kim − *Department of Chemistry, Yonsei University, Seoul 03722, Republic of Korea;* orcid.org/0000-0002-6419-3054; Email: bskim19@yonsei.ac.kr

Authors

Iloh Son − *Department of Chemistry, Yonsei University, Seoul 03722, Republic of Korea*

Yujin Lee − *Department of PolymerNano Science and Technology, Chonbuk National University, Jeonju 54896, Republic of Korea*

Jinsu Baek − *Department of Chemistry, Yonsei University, Seoul 03722, Republic of Korea*

Miran Park − *Department of PolymerNano Science and Technology, Chonbuk National University, Jeonju 54896, Republic of Korea;* orcid.org/0000-0001-7665-800X

Daeho Han − *Department of Chemistry, Ulsan National Institute of Science and Technology (UNIST), Ulsan 44919, Republic of Korea*

Seung Kyu Min − *Department of Chemistry, Ulsan National Institute of Science and Technology (UNIST), Ulsan 44919, Republic of Korea;* orcid.org/0000-0001-5636-3407

Dongwon Lee − *Department of PolymerNano Science and Technology, Chonbuk National University, Jeonju 54896, Republic of Korea;* orcid.org/0000-0003-3035-6342

Complete contact information is available at: https://pubs.acs.org/10.1021/acs.biomac.1c00163

https://doi.org/10.1021/acs.biomac.1c00163
Biomacromolecules 2021, 22, 2043−2056

Notes

The authors declare no competing financial interest.

■ ACKNOWLEDGMENTS

This work was supported by the National Research Foundation of Korea (NRF-2021R1A2C3004978) and the Yonsei University Research Fund of 2020 (2020-22-0494).

■ REFERENCES

(1) Delplace, V.; Couvreur, P.; Nicolas, J. Recent Trends in the Design of Anticancer Polymer Prodrug Nanocarriers. *Polym. Chem.* **2014**, *5*, 1529−1544.
(2) Fleige, E.; Quadir, M. A.; Haag, R. Stimuli-Responsive Polymeric Nanocarriers for the Controlled Transport of Active Compounds: Concepts and Applications. *Adv. Drug Delivery Rev.* **2012**, *64*, 866−884.
(3) Cho, K.; Wang, X.; Nie, S.; Chen, Z. (. G.).; Shin, D. M. Therapeutic Nanoparticles for Drug Delivery in Cancer. *Clin. Cancer Res.* **2008**, *14*, 1310−1316.
(4) Du, J. Z.; Du, X. J.; Mao, C. Q.; Wang, J. Tailor-Made Dual pH-Sensitive Polymer-Doxorubicin Nanoparticles for Efficient Anticancer Drug Delivery. *J. Am. Chem. Soc.* **2011**, *133*, 17560−17563.
(5) Hu, X.; Hu, J.; Tian, J.; Ge, Z.; Zhang, G.; Luo, K.; Liu, S. Polyprodrug Amphiphiles: Hierarchical Assemblies for Shape-Regulated Cellular Internalization, Trafficking, and Drug Delivery. *J. Am. Chem. Soc.* **2013**, *135*, 17617−17629.
(6) Chen, G.; Roy, I.; Yang, C.; Prasad, P. N. Nanochemistry and Nanomedicine for Nanoparticle-Based Diagnostics and Therapy. *Chem. Rev.* **2016**, *116*, 2826−2885.
(7) Allen, C.; Han, J.; Yu, Y.; Maysinger, D.; Eisenberg, A. Polycaprolactone-*b*-Poly(ethylene oxide) Copolymer Micelles as a Delivery Vehicle for Dihydrotestosterone. *J. Controlled Release* **2000**, *63*, 275−286.
(8) Lu, J.; Owen, S. C.; Shoichet, M. S. Stability of Self-Assembled Polymeric Micelles in Serum. *Macromolecules* **2011**, *44*, 6002−6008.
(9) Ding, J.; Chen, L.; Xiao, C.; Chen, L.; Zhuang, X.; Chen, X. Noncovalent Interaction-Assisted Polymeric Micelles for Controlled Drug Delivery. *Chem. Commun.* **2014**, *50*, 11274−11290.
(10) Zhao, X.; Poon, Z.; Engler, A. C.; Bonner, D. K.; Hammond, P. T. Enhanced Stability of Polymeric Micelles Based on Postfunctionalized Poly(ethylene glycol)-*b*-Poly(γ-propargyl L-glutamate): The Substituent Effect. *Biomacromolecules* **2012**, *13*, 1315−1322.
(11) Li, M.; Song, W.; Tang, Z.; Lv, S.; Lin, L.; Sun, H.; Li, Q.; Yang, Y.; Hong, H.; Chen, X. Nanoscaled Poly(l-glutamic acid)/Doxorubicin-Amphiphile Complex as pH-Responsive Drug Delivery System for Effective Treatment of Nonsmall Cell Lung Cancer. *ACS Appl. Mater. Interfaces* **2013**, *5*, 1781−1792.
(12) Zhang, J.; Ma, P. X. Polymeric Core-Shell Assemblies Mediated by Host-Guest Interactions: Versatile Nanocarriers for Drug Delivery. *Angew. Chem., Int. Ed.* **2009**, *48*, 964−968.
(13) Kim, S. H.; Tan, J. P. K.; Nederberg, F.; Fukushima, K.; Colson, J.; Yang, C.; Nelson, A.; Yang, Y.-Y.; Hedrick, J. L. Hydrogen Bonding-Enhanced Micelle Assemblies for Drug Delivery. *Biomaterials* **2010**, *31*, 8063−8071.
(14) Chung, H. J.; Park, T. G. Self-Assembled and Nanostructured Hydrogels for Drug Delivery and Tissue Engineering. *Nano Today* **2009**, *4*, 429−437.
(15) Cabral, H.; Matsumoto, Y.; Mizuno, K.; Chen, Q.; Murakami, M.; Kimura, M.; Terada, Y.; Kano, M. R.; Miyazono, K.; Uesaka, M.; Nishiyama, N.; Kataoka, K. Accumulation of Sub-100 nm Polymeric Micelles in Poorly Permeable Tumours Depends on Size. *Nat. Nanotechnol.* **2011**, *6*, 815−823.
(16) Li, J.; Huo, M.; Wang, J.; Zhou, J.; Mohammad, J. M.; Zhang, Y.; Zhu, Q.; Waddad, A. Y.; Zhang, Q. Redox-sensitive Micelles Self-Assembled from Amphiphilic Hyaluronic Acid-Deoxycholic Acid Conjugates for Targeted Intracellular Delivery of Paclitaxel. *Biomaterials* **2012**, *33*, 2310−2320.
(17) Du, Y.-Z.; Weng, Q.; Yuan, H.; Hu, F.-Q. Synthesis and Antitumor Activity of Stearate-*g*-Dextran Micelles for Intracellular Doxorubicin Delivery. *ACS Nano* **2010**, *4*, 6894−6902.
(18) Ke, X.; Ng, V. W. L.; Ono, R. J.; Chan, J. M. W.; Krishnamurthy, S.; Wang, Y.; Hedrick, J. L.; Yang, Y. Y. Role of Non-Covalent and Covalent Interactions in Cargo Loading Capacity and Stability of Polymeric Micelles. *J. Controlled Release* **2014**, *193*, 9−26.
(19) Blum, A. P.; Kammeyer, J. K.; Rush, A. M.; Callmann, C. E.; Hahn, M. E.; Gianneschi, N. C. Stimuli-Responsive Nanomaterials for Biomedical Applications. *J. Am. Chem. Soc.* **2015**, *137*, 2140−2154.
(20) Kanamala, M.; Wilson, W. R.; Yang, M.; Palmer, B. D.; Wu, Z. Mechanisms and Biomaterials in pH-Responsive Tumour Targeted Drug Delivery: A Review. *Biomaterials* **2016**, *85*, 152−167.
(21) Warburg, O. The Metabolism of Carcinoma Cells. *J. Cancer Res.* **1925**, *9*, 148.
(22) Rajamäki, K.; Nordström, T.; Nurmi, K.; Åkerman, K. E. O.; Kovanen, P. T.; Öörni, K.; Eklund, K. K. Extracellular Acidosis Is a Novel Danger Signal Alerting Innate Immunity via the NLRP3 Inflammasome. *J. Biol. Chem.* **2013**, *288*, 13410−13419.
(23) Lee, S. J.; Min, K. H.; Lee, H. J.; Koo, A. N.; Rim, H. P.; Jeon, B. J.; Jeong, S. Y.; Heo, J. S.; Lee, S. C. Ketal Cross-Linked Poly(ethylene glycol)-Poly(amino acid)s Copolymer Micelles for Efficient Intracellular Delivery of Doxorubicin. *Biomacromolecules* **2011**, *12*, 1224−1233.
(24) Cao, H.; Chen, C.; Xie, D.; Chen, X.; Wang, P.; Wang, Y.; Song, H.; Wang, W. A Hyperbranched Amphiphilic Acetal Polymer for pH-Sensitive Drug Delivery. *Polym. Chem.* **2018**, *9*, 169−177.
(25) Long, Y.-B.; Gu, W.-X.; Pang, C.; Ma, J.; Gao, H. Construction of Coumarin-Based Cross-Linked Micelles with pH Responsive Hydrazone Bond and Tumor Targeting Moiety. *J. Mater. Chem. B* **2016**, *4*, 1480−1488.
(26) Luo, L.; Xu, F.; Peng, H.; Luo, Y.; Tian, X.; Battaglia, G.; Zhang, H.; Gong, Q.; Gu, Z.; Luo, K. Stimuli-Responsive Polymeric Prodrug-Based Nanomedicine Delivering Nifuroxazide and Doxorubicin against Primary Breast Cancer and Pulmonary Metastasis. *J. Controlled Release* **2020**, *318*, 124−135.
(27) Long, M.; Liu, S.; Shan, X.; Mao, J.; Yang, F.; Wu, X.; Qiu, L.; Chen, J. Self-Assembly of pH-Sensitive Micelles for Enhanced Delivery of Doxorubicin to Melanoma Cells. *J. Drug Delivery Sci. Technol.* **2020**, *59*, 101859.
(28) Jazani, A. M.; Oh, J. K. Development and Disassembly of Single and Multiple Acid-Cleavable Block Copolymer Nanoassemblies for Drug Delivery. *Polym. Chem.* **2020**, *11*, 2934−2954.
(29) Hwang, E.; Kim, K.; Lee, C. G.; Kwon, T.-H.; Lee, S.-H.; Min, S. K.; Kim, B.-S. Tailorable Degradation of pH-Responsive All-Polyether Micelles: Unveiling the Role of Monomer Structure and Hydrophilic−Hydrophobic Balance. *Macromolecules* **2019**, *52*, 5884−5893.
(30) Song, J.; Palanikumar, L.; Choi, Y.; Kim, I.; Heo, T.-y.; Ahn, E.; Choi, S.-H.; Lee, E.; Shibasaki, Y.; Ryu, J.-H.; Kim, B.-S. The Power of the Ring: A pH-Responsive Hydrophobic Epoxide Monomer for Superior Micelle Stability. *Polym. Chem.* **2017**, *8*, 7119−7132.
(31) Satoh, Y.; Miyachi, K.; Matsuno, H.; Isono, T.; Tajima, K.; Kakuchi, T.; Satoh, T. Synthesis of Well-Defined Amphiphilic Star-Block and Miktoarm Star Copolyethers via *t*-Bu-P_4-Catalyzed Ring-Opening Polymerization of Glycidyl Ethers. *Macromolecules* **2016**, *49*, 499−509.
(32) Tetko, I. V.; Gasteiger, J.; Todeschini, R.; Mauri, A.; Livingstone, D.; Ertl, P.; Palyulin, V. A.; Radchenko, E. V.; Zefirov, N. S.; Makarenko, A. S.; Tanchuk, V. Y.; Prokopenko, V. V. Virtual Computational Chemistry Laboratory–Design and Description. *J. Comput.-Aided Mol. Des.* **2005**, *19*, 453−463.
(33) Batrakova, E. V.; Li, S.; Li, Y.; Alakhov, V. Y.; Elmquist, W. F.; Kabanov, A. V. Distribution Kinetics of a Micelle-Forming Block Copolymer Pluronic P85. *J. Controlled Release* **2004**, *100*, 389−397.
(34) Liu, J.; Zeng, F.; Allen, C. In Vivo Fate of Unimers and Micelles of a Poly(ethylene glycol)-*block*-Poly(caprolactone) Copolymer in

https://doi.org/10.1021/acs.biomac.1c00163
Biomacromolecules 2021, 22, 2043−2056

Mice Following Intravenous Administration. *Eur. J. Pharm. Biopharm.* **2007**, *65*, 309−319.
(35) Ndou, T. T.; von Wandruszka, R. Pyrene Fluorescence in Premicellar Solutions: The Effects of Solvents and Temperature. *J. Lumin.* **1990**, *46*, 33−38.
(36) Wilhelm, M.; Zhao, C. L.; Wang, Y.; Xu, R.; Winnik, M. A.; Mura, J. L.; Riess, G.; Croucher, M. D. Poly(styrene-ethylene oxide) Block Copolymer Micelle Formation in Water: A Fluorescence Probe Study. *Macromolecules* **1991**, *24*, 1033−1040.
(37) Huang, L.; Cai, M.; Xie, X.; Chen, Y.; Luo, X. Uptake Enhancement of Curcumin Encapsulated into Phosphatidylcholine-Shielding Micelles by Cancer Cells. *J. Biomater. Sci., Polym. Ed.* **2014**, *25*, 1407−1424.
(38) Wolf, F. K.; Hofmann, A. M.; Frey, H. Poly(isoglycerol methacrylate)-*b*-Poly(D or L-lactide) Copolymers: A Novel Hydrophilic Methacrylate as Building Block for Supramolecular Aggregates. *Macromolecules* **2010**, *43*, 3314−3324.
(39) Rijcken, C. J.; Snel, C. J.; Schiffelers, R. M.; van Nostrum, C. F.; Hennink, W. E. Hydrolysable Core-Crosslinked Thermosensitive Polymeric Micelles: Synthesis, Characterisation and in Vivo Studies. *Biomaterials* **2007**, *28*, 5581−5593.
(40) Koo, A. N.; Lee, H. J.; Kim, S. E.; Chang, J. H.; Park, C.; Kim, C.; Park, J. H.; Lee, S. C. Disulfide-Cross-Linked PEG-Poly(amino acid)s Copolymer Micelles for Glutathione-Mediated Intracellular Drug Delivery. *Chem. Commun.* **2008**, 6570−6572.
(41) Xie, M.; Wang, S.; Singh, A.; Cooksey, T. J.; Marquez, M. D.; Bhattarai, A.; Kourentzi, K.; Robertson, M. L. Fluorophore Exchange Kinetics in Block Copolymer Micelles with Varying Solvent-Fluorophore and Solvent-Polymer Interactions. *Soft Matter* **2016**, *12*, 6196−6205.
(42) Brock, D. J.; Kondow-McConaghy, H. M.; Hager, E. C.; Pellois, J. P. Endosomal Escape and Cytosolic Penetration of Macromolecules Mediated by Synthetic Delivery Agents. *Bioconjugate Chem.* **2019**, *30*, 293−304.
(43) Seong, K.; Seo, H.; Ahn, W.; Yoo, D.; Cho, S.; Khang, G.; Lee, D. Enhanced Cytosolic Drug Delivery Using Fully Biodegradable Poly(amino oxalate) Particles. *J. Controlled Release* **2011**, *152*, 257−263.
(44) Bus, T.; Traeger, A.; Schubert, U. S. The Great Escape: How Cationic Polyplexes Overcome the Endosomal Barrier. *J. Mater. Chem. B* **2018**, *6*, 6904−6918.
(45) Ozer, J.; Ratner, M.; Shaw, M.; Bailey, W.; Schomaker, S. The Current State of Serum Biomarkers of Hepatotoxicity. *Toxicology* **2008**, *245*, 194−205.
(46) Yang, W.; Noh, J.; Park, H.; Gwon, S.; Singh, B.; Song, C.; Lee, D. Near Infrared Dye-Conjugated Oxidative Stress Amplifying Polymer Micelles for Dual Imaging and Synergistic Anticancer Phototherapy. *Biomaterials* **2018**, *154*, 48−59.
(47) Noh, J.; Jung, E.; Lee, J.; Hyun, H.; Hong, S.; Lee, D. Engineered Polymeric Micelles for Combinational Oxidation Anticancer Therapy through Concurrent HO-1 Inhibition and ROS Generation. *Biomacromolecules* **2019**, *20*, 1109−1117.

https://doi.org/10.1021/acs.biomac.1c00163
Biomacromolecules 2021, 22, 2043−2056